

Research paper

Controlling the mechanical behaviour of stochastic lattice structures: The key role of nodal connectivity

Stylianos Kechagias, Reece N. Oosterbeek, Maxwell J. Munford, Shaaz Ghouse, Jonathan R. T. Jeffers^{*}

Department of Mechanical Engineering, Imperial College London, SW7 2AZ London, United Kingdom

ARTICLE INFO

Keywords:

Lattice structures
Bone scaffolds
Connectivity
Topology
Fatigue life

ABSTRACT

Additive manufacturing has enabled the fabrication of lattice structures with controlled micro-architectures and mechanical properties. These structures are particularly attractive in the orthopaedic industry where their osseointegration capability and bone-matching mechanical properties are ideally suited for use in implants and bone scaffolds. The broad range of mechanical properties required for this application is a challenge – it typically requires a range of periodic lattice structures, each of which require separate characterisation. An alternative approach is to use a stochastic lattice structure, where a single relationship between the lattice design parameters (connectivity, strut density and strut thickness) and resulting mechanical properties should be possible. To investigate this, we manufactured stochastic lattices in pure Titanium with connectivity from 4 to 14, strut density from 3 to 7 [struts/mm³] and strut thickness of 230 and 300 μm. Specimens were compression tested in quasi-static and fatigue loading. In static loading, the low connectivity structures displayed bend-dominated deformation while the high connectivity structures displayed stretch-dominated deformation. The structures had a stiffness ranging from 0.1 to 8 GPa and different Gibson-Ashby stiffness/relative density relationships were required for high and low connectivity structures. A unified multivariable linear regression model was found to predict relative density from the connectivity, strut density and strut thickness of the structure. In fatigue loading, increasing the connectivity from 4 to 14 increased the fatigue strength by 60% for a fixed relative density. These findings provide important design information when creating structures using stochastic lattices to maximise strength for a desired relative density or stiffness. The single integrated model presented in this study can define a structure to achieve a broad range of design requirements, even as gradient within the same component. To achieve the same with periodic lattices would require different unit cell, with individual regression models for each unit cell used.

1. Introduction

Cellular materials found in nature, like cancellous bone, wood, and cork, have inspired the development of metal, polymer and ceramic artificial structures which combine advanced mechanical, optical or thermal properties through their micro-architecture [1,2]. Although formed from numerous inter-connected cells, these artificial structures exhibit unified properties which differ from the properties of their parent material [3]. Initially, they were mainly fabricated through conventional manufacturing methods, such as gas foaming and solvent casting [4], which produce foams with randomly distributed open or closed pores. Advancement of computer-aided design (CAD) and additive manufacturing (AM), however, enables the fabrication of 3D lattices

with fully controllable micro-architectures and properties. Lattices constitute inter-connected networks of beams/struts or sheets/plates [3, 5] with various industrial applications in lightweight structures, energy absorbers, heat exchangers and orthopaedic implants as bone regeneration scaffolds [6].

The properties of artificial cellular materials are determined by three factors: the (parent) material from which they are made of, their relative density, and their topology [1]. Relative density is the ratio of structure's physical density ρ to parent material's density ρ_s , and it is typically regulated through cell size and strut thickness/diameter [7,8]. Topology refers to nodal connectivity Z (number of struts connected to a node) and the shape of structure's cells. Although cell geometry and topology are not clear in case of foams, they are fully controllable in AM

^{*} Corresponding author

E-mail address: j.jeffers@imperial.ac.uk (J.R.T. Jeffers).

<https://doi.org/10.1016/j.addma.2022.102730>

Received 20 December 2021; Received in revised form 17 February 2022; Accepted 2 March 2022

Available online 4 March 2022

2214-8604/© 2022 The Authors. Published by Elsevier B.V. This is an open access article under the CC BY license (<http://creativecommons.org/licenses/by/4.0/>).

lattices. Depending on their micro-architecture, lattices can be periodic or non-periodic (also termed as stochastic).

Periodic structures are widely studied and increased connectivity is reported to increase stiffness, quasi-static strength [9–12] and fatigue strength [13,14]. This is usually attributed to internal loads developed in structures' struts, resulting in different deformation modes. High connectivity structures exhibit stretching-dominated behaviour due to the development of axial loads in their struts making them more rigid. While, low connectivity structures appear to be more compliant due to their struts' tendency to bend under external loading (bending-dominated behaviour) [1]. The Maxwell criterion¹ can be used to identify the type of deformation mode by examining the whole structure or its structural unit cell (structures built from rigid unit cells will also be rigid). For a 3D periodic structure, nodal connectivity of at least 12 has been shown to be necessary for stretching-dominated behaviour [15].

Less data exists for stochastic structures, but the stochastic approach is particularly suited to manufacturing lattice parts that form irregular geometry, have curved surfaces, or where the hidden planes of anisotropy of periodic structures (due to the repeated struts orientated to distinct angles) is a problem [16,17]. Early studies on foams have shown that they exhibit bending-dominated behaviour, as weak areas in their heterogeneous pore network tend to reduce the mechanical properties of the whole structure [1]. For more controlled stochastic structures, Mueller et al. [18] carried out a computational analysis with stochastic lattices employing connectivity from 4 to 14 but did not find a transition from a bending-dominated to a stretching-dominated behaviour with increasing connectivity. In an experimental work, Raghavendra et al. [19] considered a connectivity between 4 and 6 and found stochastic structures had inferior mechanical properties (under both quasi-static and fatigue loading) compared to periodic lattices, something that was attributed to the bending-dominated behaviour of the stochastic structures.

These limited data indicate a clear need for understanding how the topology of stochastic structures affects the stretch/bend dominated behaviour and thereby the mechanical properties. A good starting point for this is the well-known Gibson-Ashby model [1,2], which correlates major mechanical properties, such as elastic modulus and (ultimate or yield) strength to relative density. Our hypothesis is that we can use three design parameters of a stochastic lattice: nodal connectivity, strut density and strut thickness to fully define the structure and correlate these to relative density. If successful, this would enable connectivity to play a key role in regulating a structure's properties, such as porosity (defined as $1 - \rho/\rho_s$), stiffness, and strength. Different properties could be achieved without being dependant solely on pore size or strut thickness which is the current state of the art. Subsequently, combining all three design parameters will enable the production of stochastic lattices with a wide range of properties using one holistic design framework – without having to choose between periodic lattices of different unit cells which require distinct models to predict their properties.

This would be useful in applications where a wide range of properties need to be combined, such as in the case of orthopaedic implants and scaffolds. These have particular requirements of porosity [20] and stiffness [21,22] that may vary throughout a single part. For example, the stiffness of bone varies from cancellous (0.05–5 GPa) to cortical (7–30 GPa) [22,23] and an implantable device may need to match this range of properties whilst providing an acceptable porosity for biological fixation through bone ingrowth [21,24,25]. Hence, this study will further discuss how the proposed design framework can be utilised to produce scaffolds with a wide range of stiffness values while

maintaining adequately high porosity (> 60%).

2. Materials and methods

2.1. Specimen design

Stochastic lattices were designed using Rhinoceros 6 (Robert McNeel & Associates) 3D modelling software by filling a cylindrical volume ($\emptyset 13\text{mm} \times 21\text{mm}$) with pseudo-randomly distributed points [17]. The points (or nodes) were then connected to each other with zero thickness lines (the struts) by defining the number of lines connected to each point (nodal connectivity Z).

A design parameter, termed as strut density d (struts/mm³), was used to assess the number of required nodes, making the design phase more rational as it can eventually be correlated to structure's density ρ . Through strut density d and specimen volume V , the number of struts s can be expressed as:

$$s = d \cdot V$$

While the needed nodes j can be calculated using the below approximation, found in [15]:

$$j \approx (2 \cdot s) / Z$$

These equations were used as a preliminary estimation of the necessary number of struts and nodes for the creation of specimens with different d and Z values. Nodes with $Z=1$, which are unavoidable especially in the outer surface, were removed since they do not contribute to structure's mechanical response and significantly lower the average connectivity of the structure.

To avoid horizontal and low angle struts, all struts with inclination angle $< 25^\circ$ with respect to the build plate were kinked by converting the sloping lines into sloping isosceles triangles with the equal angles being 25° [17]. Additionally, vertical supporting struts were placed at the bottom surface of each cylinder to ensure that the actual height of specimens would be close to the nominal value after their removal from the substrate plate.

Twelve designs were created using different combinations of connectivity Z and strut density d with their structural properties summarised in Table 1. In-house software was used to generate slice data and assign laser parameters from CAD-based line representations [21]. Two nominal values of strut thickness were used, namely: 230 and 300 μm . The design and manufacturing workflow is depicted in Fig. 1.

2.2. Manufacturing process

Lattice structures were fabricated using an AM250 metal powder bed fusion system (Renishaw plc., UK) and commercially pure titanium Grade 2 powder with particle size range of 10–45 μm (D50: 27 μm). A contour laser scanning strategy was used with 70 μm contour diameter, 50 μm point distance, and 50 μm layer thickness. Strut thickness was

Table 1
Specimen design parameters as calculated in the 3D model.

Average nodal connectivity Z	Strut density d (struts/mm ³)	Maxwell number M	Strut length L (μm) [mean \pm S.D.]
4.0	3.0	-4291	910.1 \pm 197.9
4.0	5.0	-6713	769.4 \pm 158.5
4.1	7.0	-8908	688.3 \pm 137.9
8.3	3.0	2302	1257.1 \pm 204.9
8.3	5.0	3898	1060.9 \pm 171.4
8.3	7.0	5433	944.9 \pm 148.0
12.0	3.0	4212	1584.9 \pm 310.1
12.1	5.0	7043	1330.7 \pm 256.1
12.2	7.0	9891	1187.2 \pm 227.5
13.9	3.0	4726	1744.0 \pm 364.5
14.0	5.0	7994	1453.4 \pm 297.4
14.1	7.0	11248	1298.1 \pm 262.9

¹ Maxwell criterion utilises the number of struts s and nodes j of a structure to characterise its deformation modes based on the value of the Maxwell number M , where $M = s - 3j + 6$. If $M < 0$, the structure is bending-dominated, while if $M \geq 0$ the structure is stretching-dominated [1].

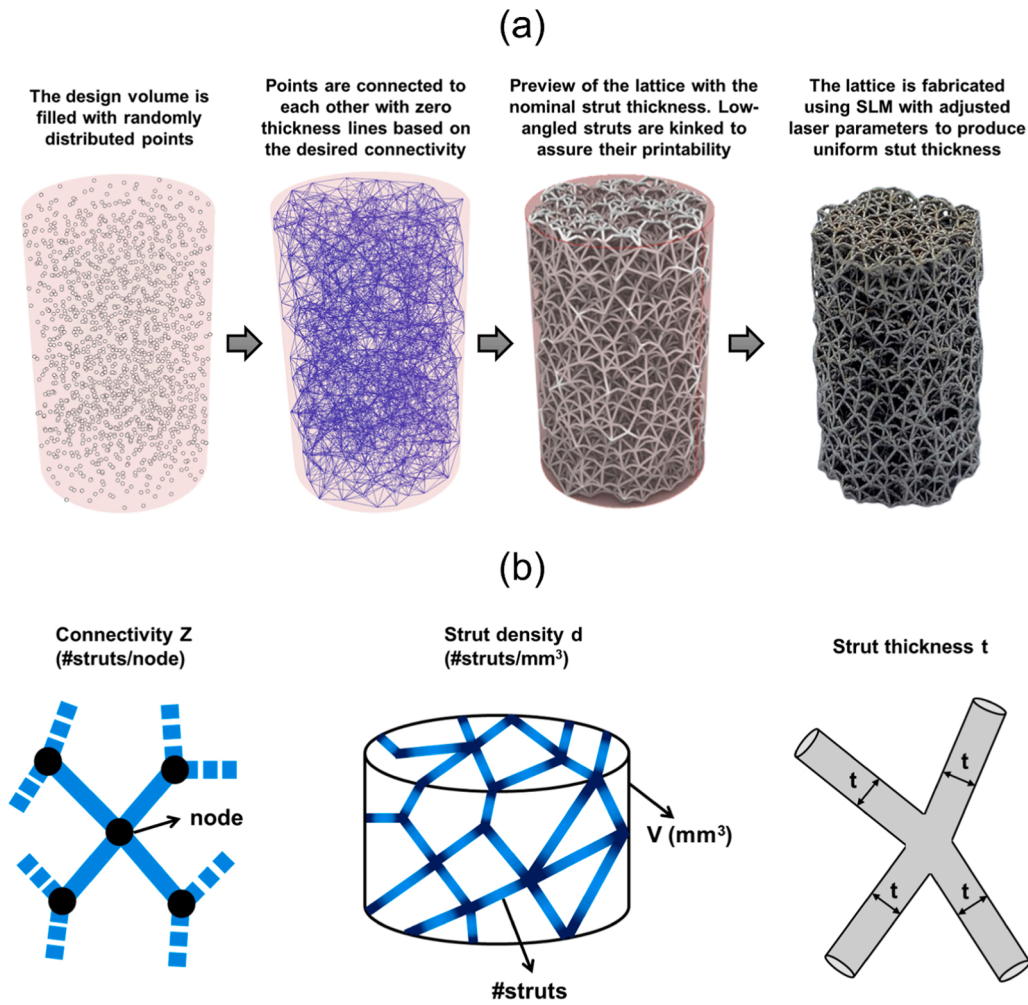


Fig. 1. (a) Design and manufacturing workflow of stochastic lattice structures. The specimen displayed was designed with connectivity $Z = 12$, strut density $d = 5$, and strut thickness $t = 230 \mu\text{m}$. (b) Sketches of the design parameters.

controlled by varying laser parameters as described in [26] (see Table S.1 in Supplementary Materials).

After printing, specimens were removed from the build plate using electro discharge machining and ground parallel to trim any supporting struts remaining. Afterward, all specimens were weighted to estimate their relative density. The density of each specimen was taken as the weight divided by the measured volume, while the density of solid CP titanium at room temperature ρ_s was taken as 4.51 g/cm^3 [27]. In total 227 specimens were mechanically tested in this study. Fig. 2.

2.3. Imaging and image processing

To inspect the thickness of the struts, one specimen per nominal strut thickness was imaged using micro-CT with a Zeiss Xradia 510 Versa (Carl Zeiss AG, Germany). From these data, the open-source software StrutSurf [28] was used to measure the thickness (diameter) of lattice struts of 20 struts of different build angles throughout the specimen volume. Scanning electron microscopy (Mira microscope, TESCAN, Czech Republic) was also used to qualitatively evaluate the morphology of the different specimens. A series of Student's t -tests were conducted to ensure that measured strut thicknesses were similar to the nominal values across different build angles and the entire sample population.

2.4. Mechanical testing

2.4.1. Quasi-Static compression

Quasi-Static compression testing was carried out in accordance with ISO 13314:2011 [29] using a uniaxial testing machine (Instron 5565 or Instron 8874) with a 5 kN, 10 kN or 25 kN load cell depending on the specimen. Specimens were centred and compressed between two parallel hardened ($> 62\text{HRC}$) lubricated platens in position control. Two linearly variable differential transformers (LVDTs) (RDP D6/05000 A) measured displacement. A preliminary specimen per combination was compressed to 9 mm ($> 40\%$ strain) at a constant strain rate of 2 mm/min to estimate the post-yield plateau stress σ_{pl} . Five specimens

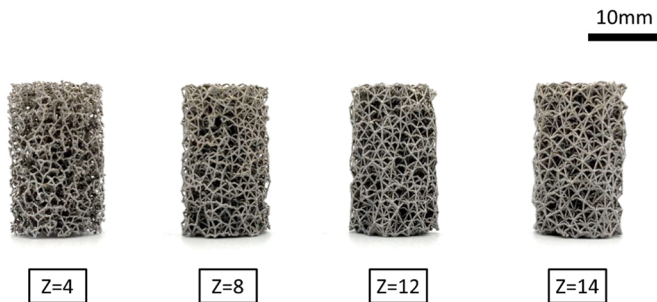


Fig. 2. Photograph of the stochastic structures manufactured with strut density $d = 3$, strut thickness $t = 230 \mu\text{m}$ and four connectivity levels Z .

per combination were subsequently compressed to 9 mm at a constant strain rate of 2 mm/min with a hysteresis loop before yield starting at 70% and reversing to 20% of σ_{pl} . The elastic modulus E was calculated as the fitted slope of the hysteresis loop (using linear regression). From the same curve, the first maximum stress point was taken as the ultimate compressive strength σ_u .

2.4.2. Cyclic compression

Compression-compression fatigue testing was carried out on specimens with four connectivity levels ($Z = 4, 8, 12, 14$), but fixed strut density ($d = 5$) and strut thickness ($t = 230 \mu\text{m}$). An additional design with $Z = 4$, $d = 5$ and $t = 300 \mu\text{m}$ was tested to isolate the effect of connectivity Z while maintaining the same relative density (21.1%) as the specimen with $Z = 14$, $d = 5$ and $t = 230 \mu\text{m}$.

Testing was performed in accordance with ISO 1099:2017 [30] using a universal testing machine (Instron 8872 or Instron 8874) with a 1 kN or 10 kN load cell depending on the applied forces. Specimens were tested in load control at a frequency of 15 Hz (sinusoidal wave form) with $R = 0.1$. Tests were terminated after 1 million cycles or when the moving platen reached 2 mm displacement ($\sim 10\%$ compressive strain). The number of cycles at 5% strain was taken as the fatigue life.

Two specimens per combination were tested at five stress levels (80%, 65%, 50%, 35%, and 25% of σ_u) to produce the S-N curves. If the fatigue life at a stress level demonstrated $> 40\%$ difference between the two measurements a third measurement was taken as proposed in [31, 32]. The modified staircase method (ISO 12107:2012 [33]) was used to find the fatigue life at 10^6 cycles with an initial stress of 20% σ_u and step size of 1.25% σ_u using 6 specimens for each combination of design parameters [34].

2.4.3. Statistical analysis

A series of statistical tests were carried out to demonstrate how the combination of the three design parameters (Z , d , t) affected the mechanical properties (ρ/ρ_s , E , σ_y) of the lattice structures. First, a three-way analysis of variance (3-way ANOVA) was conducted to prove that each design parameter as well as their combination independently affect each one of the three examined mechanical properties. Hence, the 3-way ANOVA was conducted three times, one for each mechanical property as the dependent variable. Then, Pearson's correlation was used to demonstrate the magnitude and direction of the potential effect of each design parameter to each mechanical property. Lastly, regression models were computed to correlate the design parameters with the resultant mechanical properties.

3. Theory

3.1. Relationship between relative density and connectivity of a structure

The following Gibson and Ashby [2] relationship is widely used to predict relative density for both periodic and stochastic porous structures of various geometries for relative densities higher than 20% when the strut thickness (t) \ll strut length (L) [2]:

$$\frac{\rho}{\rho_s} = C \left(\frac{t}{L} \right)^2 + D \left(\frac{t}{L} \right)^3$$

Where, ρ is the density of the structure, ρ_s is the density of the parent material, C and D are constants of proportionality calculated using experimental data. This relationship is used to investigate whether connectivity affects the relative density – this should be apparent with different values of C and D for different connectivity structures.

3.2. Relationship between mechanical properties under uniaxial compression

Gibson and Ashby further correlated relative density to the

compressive strength σ_u and elastic modulus E , when a lattice fails under yielding, through the power law relationships below [1,2]:

$$\frac{\sigma_u}{\sigma_{ys}} = C_1 \left(\frac{\rho}{\rho_s} \right)^n$$

$$\frac{E}{E_s} = C_2 \left(\frac{\rho}{\rho_s} \right)^m$$

Where σ_{ys} and E_s denote the yield strength and the elastic modulus of solid parent material, respectively. The values of power indices n and m depend on the deformation mode. Based on the theoretical model, the index n should be equal to 1.5 and 1 for bending-dominated and stretching-dominated structures, respectively. While the index m should be equal to 2 and 1 for bending-dominated and stretching-dominated structures, respectively. However, previously published results have shown that n and m values might lie between, below or above the theoretical values regardless of structures' deformation behaviour based on the Maxwell criterion [5]. Despite its limitations, this set of equations constitutes a useful tool for lightweight applications, where structures are designed to have high strength with the lowest possible density. However, when designing a scaffold for orthopaedic surgery, maximising strength in terms of stiffness (elastic modulus) is more critical. By combining these two equations, a modified expression of Gibson-Ashby model can be obtained [26]:

$$\frac{\sigma_u}{\sigma_{ys}} = C_3 \left(\frac{E}{E_s} \right)^{n/m}$$

This relationship is used to compare the strength to stiffness ratio for all the structures manufactured in this study and also to compare to previously reported lattice structures.

4. Results

4.1. Structural and morphological evaluation of manufactured specimens

The measured thicknesses of struts with nominal thicknesses of 230 μm and 300 μm were $227.8 \pm 10.5 \mu\text{m}$ and $305.4 \pm 16.9 \mu\text{m}$, respectively. Measured thicknesses were the same as the nominal values (p -values > 0.05) for all inclination angles (data can be found in Table S.2 at Supplementary Materials).

The relationship between relative density ρ/ρ_s and strut thickness/length ratio t/L is shown in Fig. 3 (data provided in Tables 1 and 2). The data shows a clear relationship between ρ/ρ_s and t/L as expected by the Gibson Ashby theory [2], however the relationship is distinctly different for different connectivity values. This outcome suggests that connectivity regulates relative density independently from the other two design parameters, and generally that topology and relative density are inextricable [2].

Valuable inferences can be drawn from SEM images regarding the morphology of the additively manufactured surfaces, representative examples are shown in Fig. 4. Firstly, struts of all angles appeared to have successfully been built for both nominal thicknesses. Secondly, defects commonly found on unsupported overhanging surfaces built via powder bed fusion were apparent in both cases. These defects consist of semi-sintered powder particles, dross formation (excessive melted material in overhanging surfaces [35]) and texture lines due to consecutive melt-pools overlapping. All the above are morphological irregularities that increase surface roughness and constitute potential crack initiation or propagation sites during cyclic loading, thus impairing the fatigue life of the structure. Furthermore, it can be observed that high connectivity nodes were bulgy with more semi-sintered particles attached to them.

4.2. Quasi-static performance

Representative stress-strain curves from the uniaxial compression of

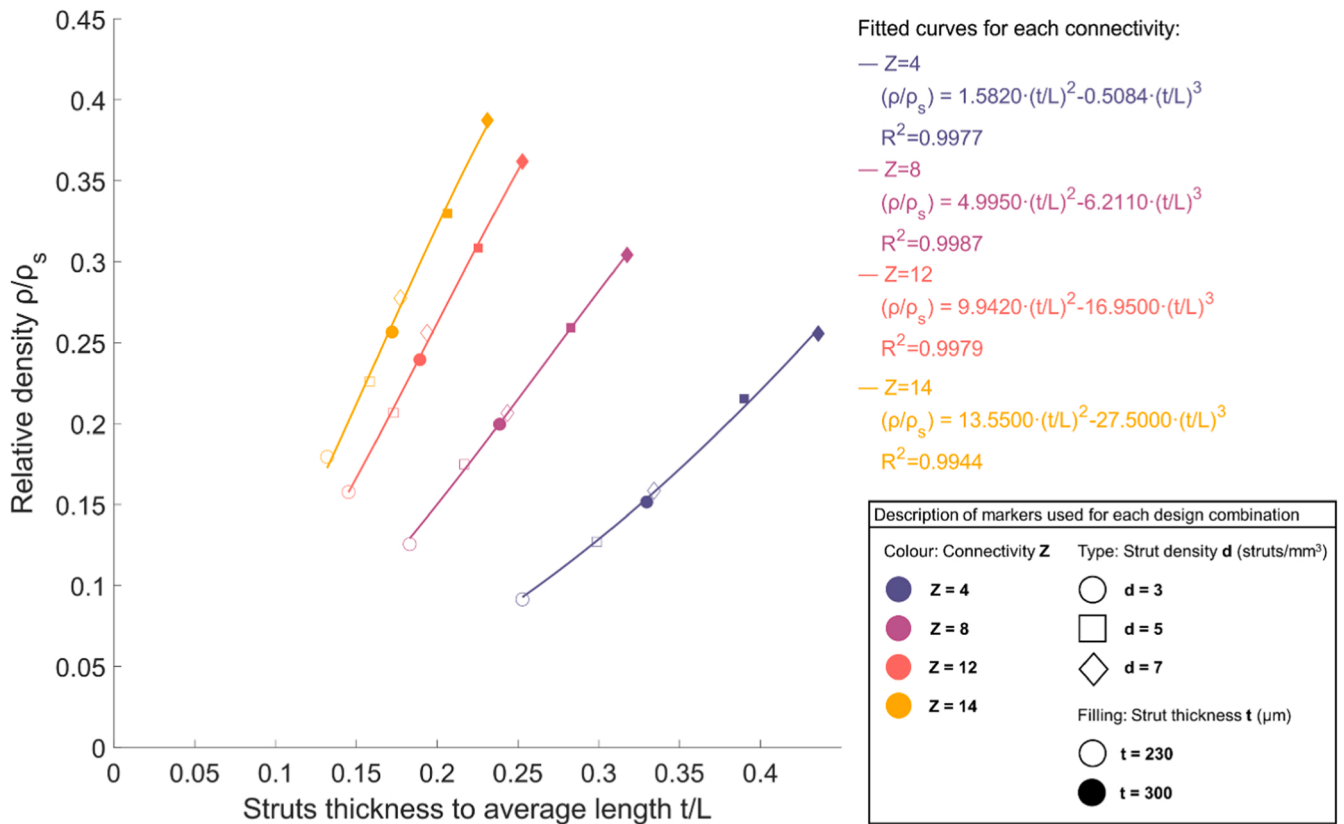


Fig. 3. The effect of strut thickness to average strut length ratio t/L on relative density ρ/ρ_s . Different regression models had to be used depending on the connectivity of the structure (each point in the graph corresponds to the average of 5 measurements).

Table 2

Measured mechanical properties for each combination of Z , d and t . Values presented as mean \pm standard deviation of the mean ($n = 5$ per combination).

Design parameters	$t = 230\mu\text{m}$			$t = 300\mu\text{m}$		
	ρ/ρ_s (%)	E [MPa]	σ_u [MPa]	ρ/ρ_s (%)	E [MPa]	σ_u [MPa]
$Z = 4 - d = 3$	9.1 ± 0.3	140.3 ± 11.0	2.2 ± 0.1	15.5 ± 0.1	529.5 ± 43.0	7.3 ± 0.3
$Z = 4 - d = 5$	12.7 ± 0.1	375.8 ± 29.1	5.5 ± 0.2	21.5 ± 0.4	1319.3 ± 77.8	16.9 ± 1.0
$Z = 4 - d = 7$	15.9 ± 0.5	605.0 ± 21.1	8.4 ± 0.2	25.6 ± 0.4	2156.8 ± 116.1	26.3 ± 0.4
$Z = 8 - d = 3$	12.6 ± 0.2	711.1 ± 42.5	8.1 ± 0.3	20.0 ± 0.4	1791.3 ± 175.2	22.0 ± 0.6
$Z = 8 - d = 5$	17.5 ± 0.3	1449.8 ± 99.2	14.5 ± 0.6	25.9 ± 0.4	3823.7 ± 138.8	41.6 ± 0.8
$Z = 8 - d = 7$	20.7 ± 0.9	2149.2 ± 149.9	22.1 ± 0.6	30.4 ± 0.7	5146.8 ± 179.4	61.5 ± 0.7
$Z = 12 - d = 3$	15.8 ± 0.4	1146.2 ± 90.9	12.6 ± 0.6	24.0 ± 0.5	2850.1 ± 153.9	32.4 ± 0.8
$Z = 12 - d = 5$	20.7 ± 0.7	2268.2 ± 121.0	22.4 ± 0.6	30.9 ± 0.3	5835.1 ± 269.5	58.5 ± 0.4
$Z = 12 - d = 7$	25.6 ± 0.6	3182.5 ± 170.3	31.3 ± 2.0	36.2 ± 0.4	7852.5 ± 370.4	88.7 ± 1.8
$Z = 14 - d = 3$	17.9 ± 0.4	1435.5 ± 126.4	14.5 ± 0.7	25.7 ± 0.4	3619.5 ± 279.6	40.3 ± 1.6
$Z = 14 - d = 5$	22.6 ± 0.4	2509.7 ± 128.1	26.2 ± 0.3	33.0 ± 0.3	6157.3 ± 361.3	67.9 ± 1.8
$Z = 14 - d = 7$	27.8 ± 0.6	3725.7 ± 108.2	38.5 ± 0.4	38.7 ± 0.4	8178.6 ± 484.4	97.9 ± 1.3

structures with different connectivity ($Z = 4, 8, 12, 14$), but fixed strut density ($d = 5$) and strut thickness ($t = 230 \mu\text{m}$) are shown in Fig. 5(a). The same data for a fixed strut thickness of $t = 300 \mu\text{m}$ is shown in Fig. 5 (b). From the graphs, it can be inferred that connectivity Z altered the mechanical behaviour of the lattice structures. Clear stretch and bend dominated characteristics are observed for lattices designed with high ($Z \geq 8$) and low ($Z = 4$) connectivity levels respectively. For high connectivity, the ultimate compressive strength and stiffness are noticeably greater than low connectivity structures. All high connectivity structures exhibited post-yield softening which was followed by a fluctuating plateau region (strain range between 20% and 30%). By contrast, low connectivity structures exhibited an almost constant plateau stress without any post-yield softening. These findings are in line with the theoretical behaviour of stretching and bending-dominated structures found in literature [1,36]. Although the magnitude of stress was

different between the $230 \mu\text{m}$ and $300 \mu\text{m}$ struts, the shape of the stress strain curves was similar for the same connectivity. These data indicate that different Z values alter the topology of stochastic lattices in a similar way to what has been demonstrated for periodic lattices [8,11,12].

Although tests were carried out until 40% strain, all high connectivity structures ($Z \geq 8$) failed at 30% strain with a diagonal shear band (Fig. 5). On the other hand, structures with $Z = 4$ failed under extended densification (macroscopically displayed as barrelling) without an apparent shear band that bisected the structures. Failure with a diagonal shear band has been reported for numerous periodic lattices (see Section 3.2), while densification and row-by-row collapse has been linked mainly to foams or low connectivity periodic lattices owing to extended bending of struts [36–38].

Measured mechanical properties from all quasi-static tests are summarised in Table 2. The p-value was below 0.05 for all the independent

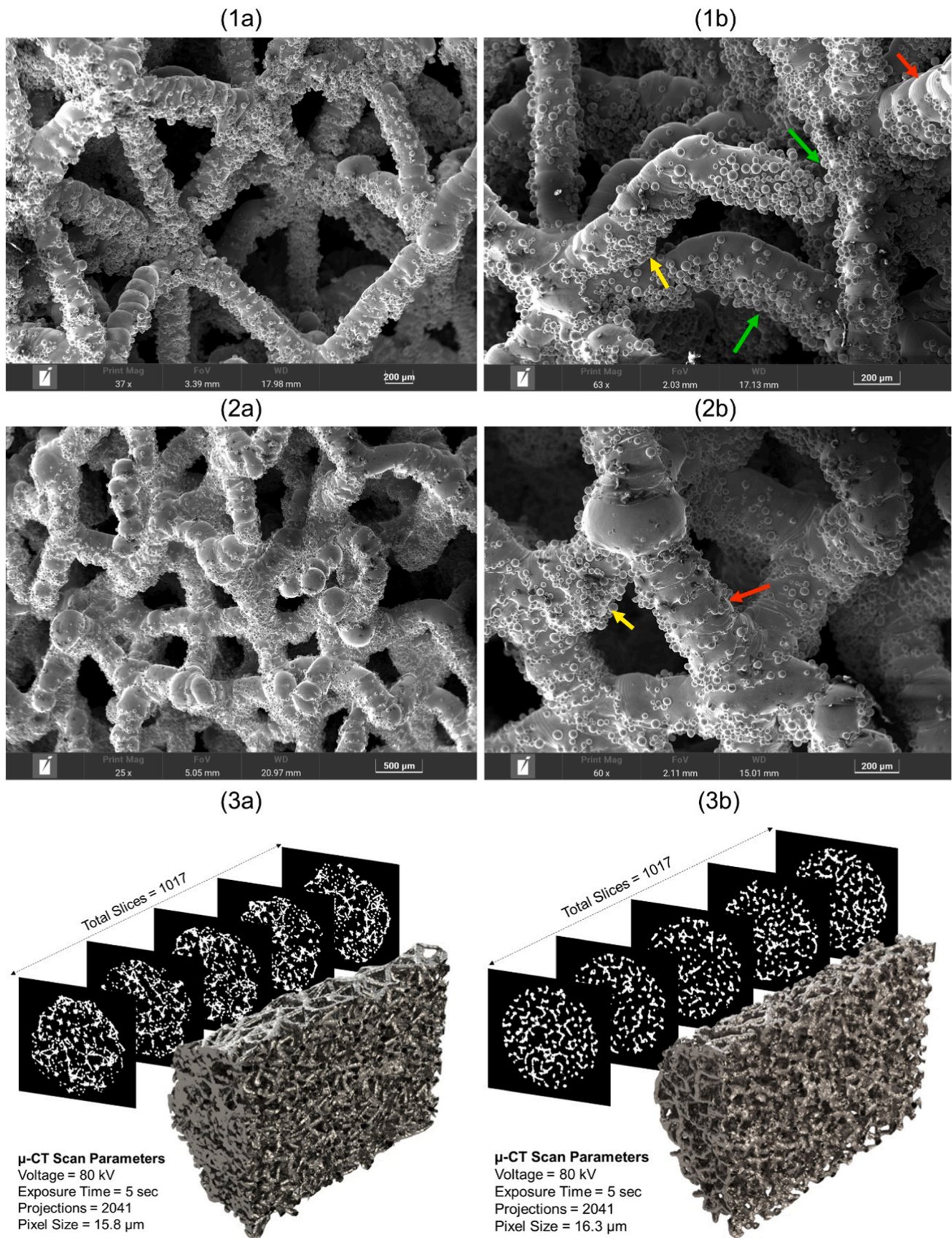


Fig. 4. SEM and μ CT images showing the morphology of AM lattice structures with (column a) $Z = 12$ and $t = 230 \mu\text{m}$ and (column b) $Z = 4$ and $t = 300 \mu\text{m}$. Magnified SEM images (row 2) demonstrate common structural defects in kinked and thick struts. Green arrows: semi-sintered particles attached to struts and nodes, yellow arrows: dross formation under the struts, red arrows: texture lines. 3D representations (row 3) of the scanned specimens demonstrate the mid-plane sections. Both imaged specimens had strut density $d = 5$. (For interpretation of the references to colour in this figure, the reader is referred to the web version of this article.)

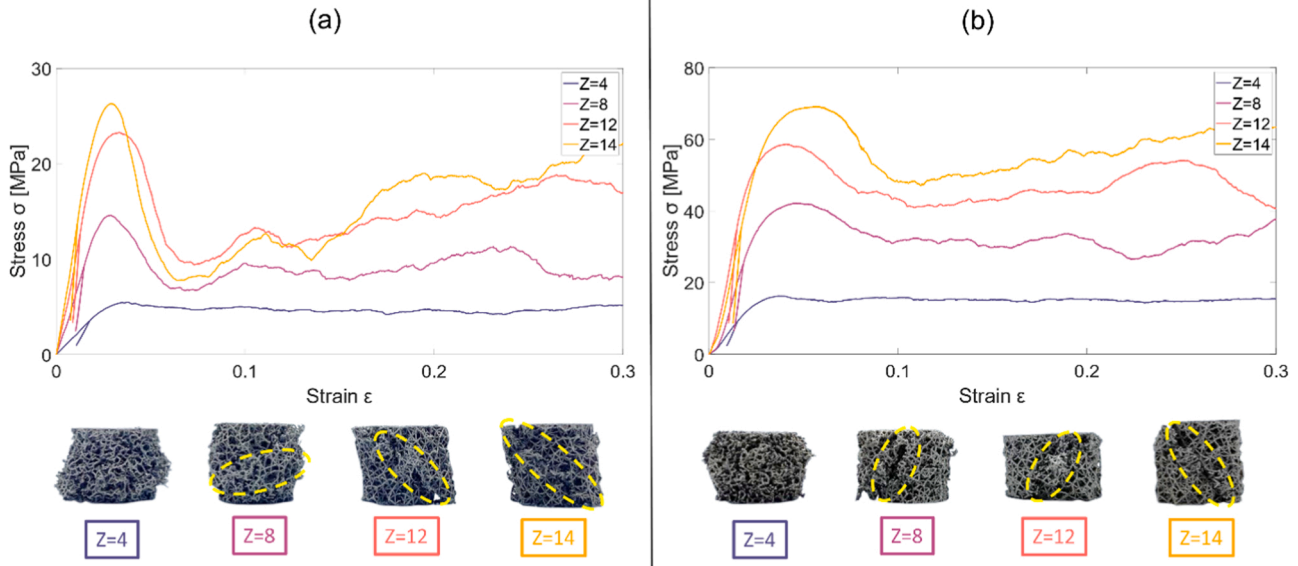


Fig. 5. The effect of different Z levels in the stress-strain curves when $d = 5$. Nominal strut thickness (a) 230 μm and (b) 300 μm . Strain up to 30% (plateau region) is displayed here. Embedded pictures demonstrate each corresponding specimen at the end of the test. Yellow ellipses indicate macroscopic crush bands in specimens with $Z \geq 8$, specimens with $Z = 4$ are found to undertake extended plastic densification leading to barrelling. (For interpretation of the references to colour in this figure, the reader is referred to the web version of this article.)

variables (connectivity, strut density, strut thickness), when examined separately and in pairs, indicating they independently influence the mechanical properties (relative density, elastic modulus, strength). Detailed statistical results can be found in Table S.3 in the [Supplementary Materials](#).

Pearson's correlation results demonstrated that all mechanical properties (relative density, elastic modulus, strength) increase with increasing connectivity, strut density and strut thickness ($r > 0.5$) (Table 3). Results also demonstrated that the three mechanical properties tend to have proportional relationship when examined pairwise ($r > 0.5$), and this interrelationship is known from the Gibson-Ashby model.

The correlations found in Table 3 indicate that a multivariable regression model can be used to correlate the three design parameters with the measured relative densities. The Gibson-Ashby model (see Section 3.1) would suggest that higher order terms might better represent the physical relationship between the design parameters and relative density. However, the different relationships between connectivity levels Z and cellular dimensions shown in Fig. 3 made it difficult for a unified relationship to be distinguished. A generic multivariable linear regression model was found adequate (adjusted $R^2 = 98.15\%$) to predict relative density using the three design parameters of this study:

$$\rho/\rho_s = 0.0110 \cdot Z + 0.0252 \cdot d + 1.29 \cdot t - 0.344$$

Where, Z corresponds to nodal connectivity [struts/node], d to strut density [struts/ mm^3], and t to strut thickness [mm]. This relationship allows the relative density of a stochastic structure (and subsequently its stiffness and strength) to be predicted when the structure is being

designed.

Power-law regression models were used to link the elastic modulus to relative density according to Gibson-Ashby (Fig. 5). Two power law fits were required to correlate elastic modulus to relative density for high ($Z \geq 8$) and low connectivity structures ($Z = 4$). The power indices m calculated for both high and low connectivity structures were > 2 , indicating all structures had bending-dominated characteristics according to the Gibson-Ashby model, contrary to what was observed from the stress-strain curves or by the Maxwell criterion (Table 1). Fig. 6.

4.3. Fatigue performance

All structures exhibited failure mechanisms which have been previously reported in compression-compression fatigue testing of both metallic foams and lattices. The initial increase in strain at the start of the test was followed by an incubation period, where crack initiation takes place, while plastic strain remained constant over increasing cycles (plateau region) (Fig. 7). The plateau region continued up to a knee point, after which plastic strain started to be accumulated rapidly until catastrophic failure. This steep increase in strain can be observed as either a vertical line with few "jumps" or as a straight vertical line [31, 38]. The former, which was exhibited in almost all structures with $Z = 4$ and in some with $Z = 8$, indicates that distinct crush bands were formed in different weak regions inside specimens' volume. The latter was found in all high connectivity structures, and indicates a uniform deformation seen as a single macroscopic crush band that extended across the diagonal of the lattice specimens.

The S-N curves and fatigue strength data are shown in Fig. 8 and Table 4 respectively. Comparing the four datasets with 230 μm thick struts, increasing the connectivity from $Z = 4$ to $Z = 14$ increased the relative density of the structures from 12.1% to 21.1%, increased the fatigue strength from 0.95 to 5.83 MPa and increased the normalised fatigue strength (σ_f/σ_y) from 0.17 to 0.22. For the two datasets with the same relative density (21.1%), the structure with $Z = 14$ had 162% of the fatigue strength of the structure with $Z = 4$, but the normalised fatigue strengths were similar. These data indicate that increasing connectivity can increase the fatigue strength of a structure for a fixed relative density (or porosity).

Table 3

Pearson's correlations for the design parameters and the measured mechanical properties. * Correlation is significant at the 0.01 level (1-tailed tests with $N = 120$).

	Independent variables (design parameters)		
	Connectivity Z	Struts density d	Struts thickness t
Relative density ρ/ρ_s	0.563 *	0.550 *	0.603 *
Elastic modulus E	0.589 *	0.470 *	0.547 *
Ultimate strength σ_u	0.544 *	0.472 *	0.581 *

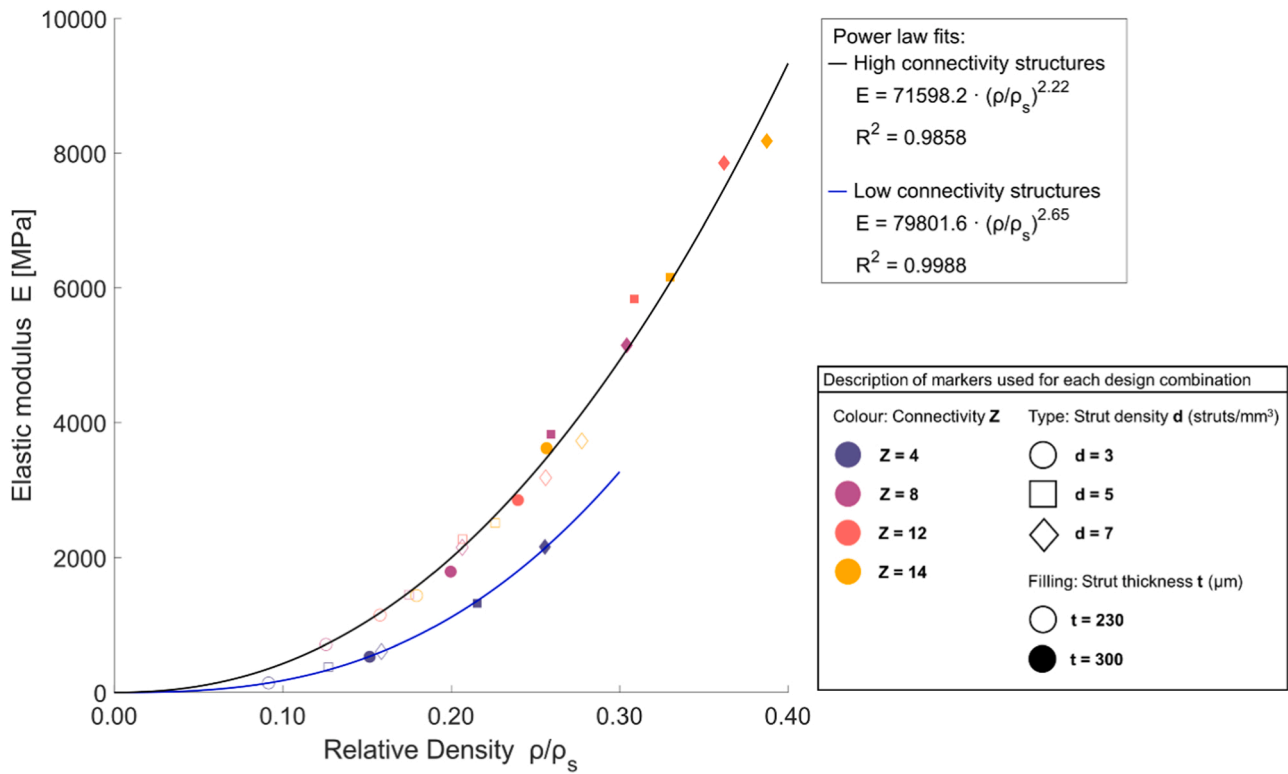


Fig. 6. Correlation of relative density to elastic modulus using the Gibson-Ashby model (each point in the graph corresponds to the average of 5 measurements).

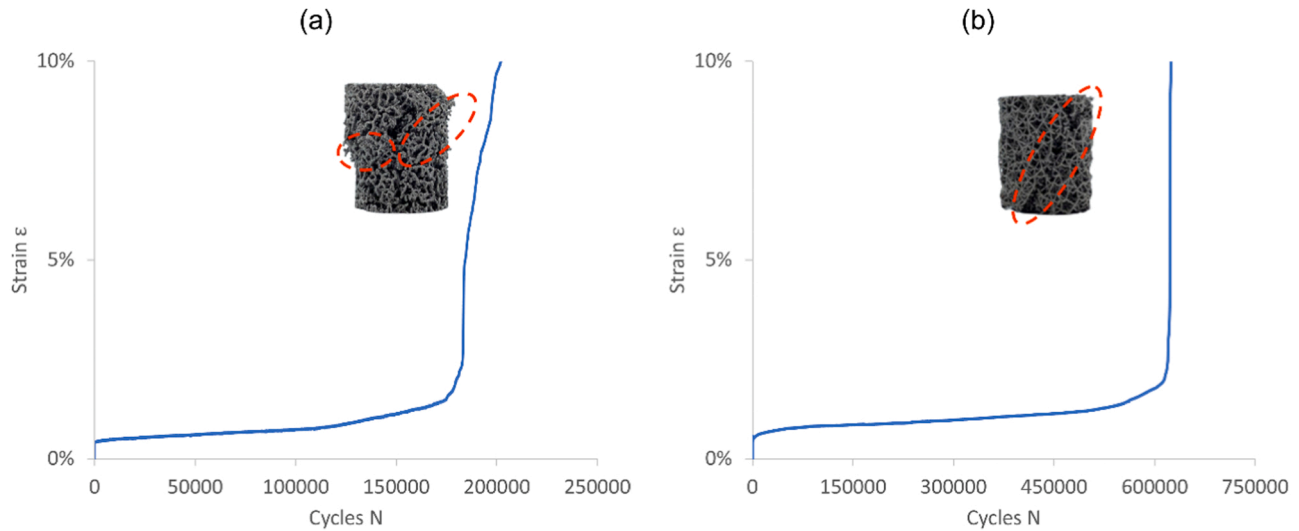


Fig. 7. Strain accumulation over fatigue cycles in lattice structures with (a) $Z = 4$ and $t = 300 \mu\text{m}$ and (b) $Z = 12$ and $t = 230 \mu\text{m}$. Embedded pictures demonstrating each specimen at the end of the test. Red ellipses indicate macroscopic crush bands which led to catastrophic failure. The test stress was 25% of the ultimate compressive strength in both structures. (For interpretation of the references to colour in this figure, the reader is referred to the web version of this article.)

5. Discussion

The most important finding of this study was that nodal connectivity Z , strut density d and strut thickness t can independently define a stochastic structure during the design phase and predict the relative density, stiffness and ultimate strength of the structure. This unified methodology was demonstrated over a wide range of porosity (60–90%) and stiffness (0.1–8 GPa). Structures with high connectivity ($Z \geq 8$) had more stretch-dominated characteristics than low connectivity ($Z = 4$) and had higher ultimate strength and stiffness for a given relative density. Connectivity was shown to independently affect relative density

and was a key parameter in fatigue loading. Increasing connectivity increased fatigue strength for a fixed relative density owing to the associated higher ultimate strength. These findings are important because they show how a stochastic lattice can be tuned to act either as a bend-dominated foam with a constant post-yield plateau, or a stretch-dominated lattice with high static and fatigue load-bearing capabilities. The advantage of the stochastic structure is that the single integrated model, presented in this study, can define the structure to achieve a broad range of design requirements, even as a gradient of properties within the same component. To achieve the same with periodic lattices would require different unit cells, with individual regression models for

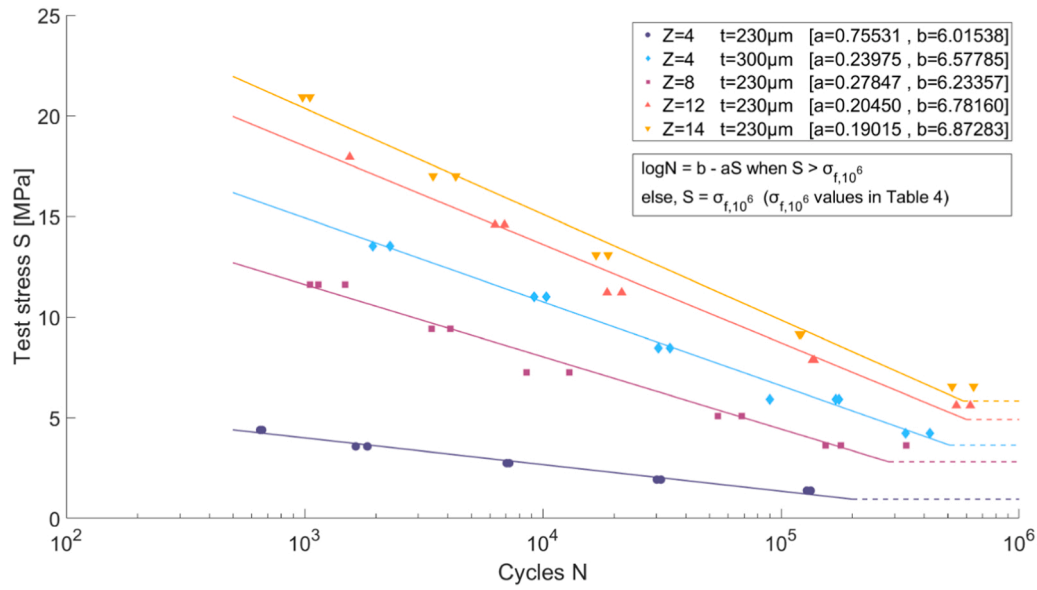


Fig. 8. S-N curves of compression-compression fatigue tests. Strut density $d = 5$ for all specimens. Dashed horizontal lines correspond to fatigue strength at 10^6 cycles, estimated using the modified staircase method ($n = 6$).

Table 4

Fatigue strength and normalised fatigue strength (σ_f/σ_u) of lattice structures. Strut density $d = 5$ for all specimens. Properties are presented as mean \pm standard deviation of the mean.

	Level of nodal connectivity Z				
	Z= 4	Z= 4	Z= 8	Z= 12	Z= 14
Nominal strut thickness (μm)	230	300	230	230	230
Relative density (%)	12.1 ± 0.3	21.1 ± 0.5	16.0 ± 0.7	19.3 ± 0.4	21.1 ± 0.8
σ_f at 10^6 cycles (MPa)	0.95 ± 0.15	3.63 ± 0.37	2.81 ± 0.16	4.91 ± 0.61	5.83 ± 0.64
Normalised σ_f at 10^6 cycles	0.17 ± 0.03	0.21 ± 0.03	0.19 ± 0.01	0.22 ± 0.03	0.22 ± 0.02

each unit cell used.

Numerous published studies can be found in literature where AM periodic lattices have been tested in quasi-static compression. Fig. 9(a) illustrates the wide range of stiffness values (100 MPa to 8 GPa) that can be manufactured from a stochastic structure that is governed by the unified relationships presented in this study – this is a wider range of values than has previously been reported in a single study. Most studies available in literature employ periodic structures made from Ti-6Al-4 V alloys, while in this study the more ductile CP-Ti was used. To allow comparison, the relationship between ultimate strength relative to the parent material and stiffness relative to the parent material are illustrated in Fig. 9(b). This comparison shows that the stochastic structures presented in the current work have an equivalent strength/modulus relationship as has been previously reported for periodic structures [11, 13,14,39,40].

Regarding fatigue testing, our normalised fatigue strength (σ_f/σ_u) of 17%–22% compared well to previous work. Normalised fatigue strength of 15–25% has been reported for Ti64 lattices with the diamond unit cell and relative densities 17–40% [41]. Normalised fatigue strength of $< 20\%$ has been reported for Ti64 lattices with the dodecahedron unit cell and relative densities from 16% to 32% [31]. In AM stochastic lattices built with Ti64, Ta and CP-Ti, normalised fatigue strength was found to range from 15% to 30% [27]. In other cases however, much higher normalised fatigue strength, between 30% and 55%, have been reported for various lattices built with both CP-Ti [13, 42] and Ti64 [43], but these estimates may not be realistic given the normalised fatigue strength of solid CP-Ti and Ti64 is $\sim 66\%$ [27] and $\sim 40\%$ [31], respectively. Overall, it seems that the tested structures

behaved comparably to what other works have shown. However, as in the case of quasi-static mechanical properties, the fatigue strength cannot be examined as an independent property. High absolute fatigue strength of a scaffold should be accompanied by a reasonable porosity and appropriate stiffness.

This study demonstrated that increased connectivity can increase fatigue strength up to 60% while maintaining constant relative density. Although it was not shown that fatigue strength can be maximised above previously reported limits, there is room for improvement. High cycle fatigue life is highly influenced by structural and morphological defects associated with AM. Semi-sintered particles and texture lines can act as stress concentration and crack initiation sites, especially near the nodes [27]. Post-processing to remove these particles and reduce strut roughness may improve the fatigue performance of stochastic lattices as suggested by literature [34,44–46].

The presented analysis has several limitations. Firstly, the anisotropy of structures was not quantitatively represented or used in the current model. Lattices used here possessed struts in all directions. The distribution of struts with respect to angle was similar for all designs: approximately 50%, 35%, and 15% of total struts corresponded to 0° – 30° , 30° – 60° and 60° – 90° angle segments in respect to the x-y plane, respectively. In previous studies where AM stochastic lattices were used [16,26,27,47], low angled struts ($< 30^\circ$) were trimmed making the structures more anisotropic and stiff along the vertical $< 0,0,1 >$ direction of uniaxial compression while employing an average connectivity of 4.5. Whilst our approach is acceptable for the uniaxial loading presented, a parameter that quantifies anisotropy could be integrated in the regression model for predicting structures' mechanical

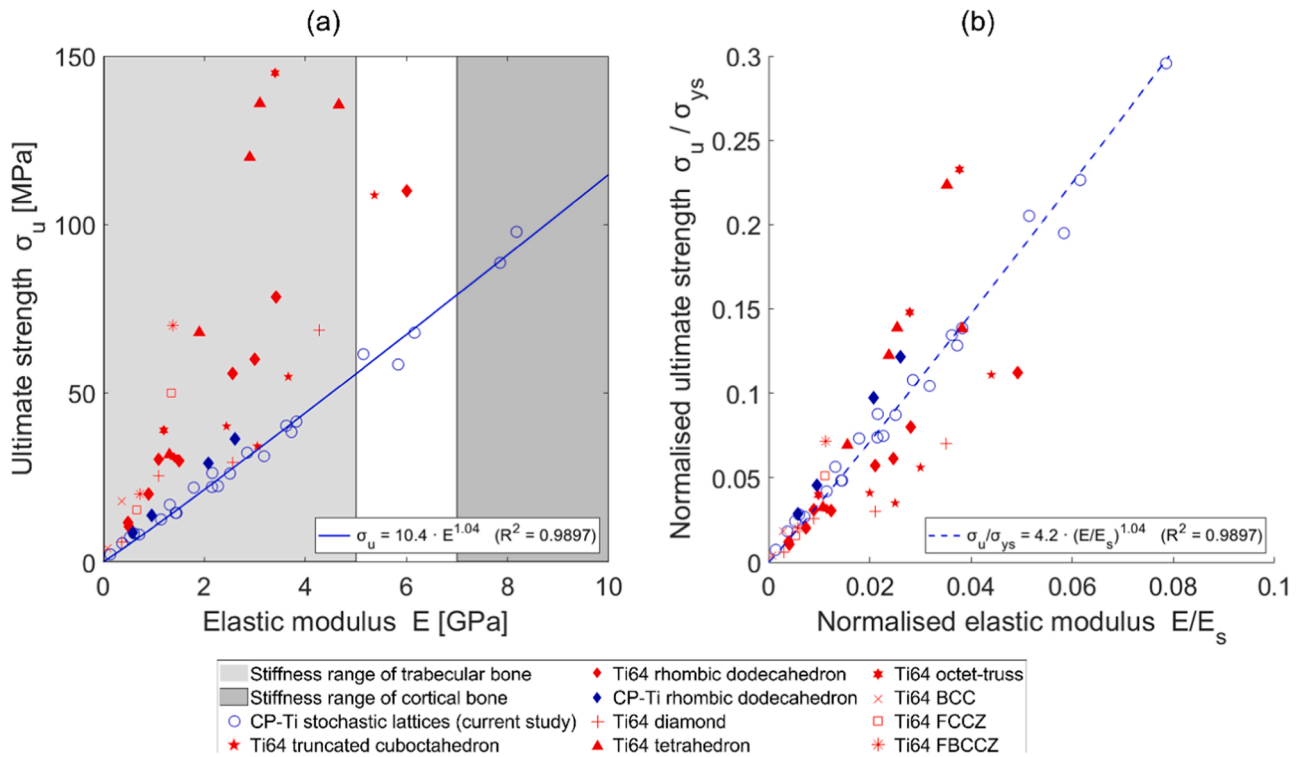


Fig. 9. Comparison of the (a) absolute and (b) normalised ultimate strength to stiffness values of previously studied CP-Ti and Ti-6Al-4 V periodic structures to the stochastic lattices of the present work. A power law regression model was used to correlate stiffness to ultimate strength using all data points from this study. Solid materials properties were taken from [11].

Data sources: [11,13,14,39,40].

properties. Secondly, only uniaxial compression tests were carried out in this study, additional tests with different loading types (tensile, bending etc.) would be beneficial for designing structures for industrial or clinical applications where structures experience multiple loading types. Thirdly, microscopy-based analysis of fractured surfaces and surface defects would lead to important information on failure mechanisms and the influence of machine parameters. We did not include this analysis in order to focus on the macroscale mechanical properties and highlight the importance of connectivity in stochastic lattice structures. Fourthly, our findings are applicable to lattice structures and may not be applicable to structures with porosity $< 60\%$ which are more indicative of solid structures with voids. Lastly, alternative ways of connecting the design parameters to a structure's properties can be investigated, for example power-law correlations. Thus, the linear relationship presented in our study may not be representative outside the range of values included in this study. However, we found a strong correlation for our linear model ($R^2 > 90\%$) indicating our approach was acceptable for the range of variables we considered.

The proposed methodology can be used in any mechanical applications to better predict mechanical behaviour at the design phase of lattice structures. In particular, we developed a methodology for the orthopaedic industry where scaffolds with variable stiffness are used to replace large cancellous bone defects [21,48], scaffolds with variable topology to mimic the morphology of natural cancellous bone [49], and scaffolds with spatially varied porosity to facilitate osseointegration [25]. Altering these properties has previously been achieved by varying strut thickness, unit cell type/size, or changing the parent material [50]. Our approach overcomes common issues, such as mismatch when connecting unit cells of different type and size, and also allows variable properties to be generated without changing the strut thickness. In practice, this is a major advantage because it requires manufacturing validation for only a single strut thickness to generate parts with the range of properties needed in the orthopaedic sector.

6. Conclusion

- This study demonstrated that stochastic lattice structures can be fully defined using three design parameters: connectivity, strut density and strut thickness.
- Out of the three design parameters that were used, connectivity was not only a porosity regulator (like strut density and strut thickness), but also a key factor for structure's mechanical behaviour and performance.
- Increasing connectivity transitioned the structure from a more compliant bending-dominated behaviour to a more rigid stretching-dominated behaviour, accompanied by a significant improvement of their quasi-static mechanical and fatigue performance.
- The single integrated model presented in this study can define a structure to achieve a broad range of design requirements, even as a gradient within the same component. To achieve the same with periodic lattices would require different unit cells, with individual regression models for each unit cell used.

CRediT authorship contribution statement

Stylianos Kechagias: Writing – original draft, Visualization, Methodology, Investigation, Formal analysis, Conceptualization. **Reece N Oosterbeek:** Writing – review & editing, Software, Methodology. **Maxwell J Munford:** Writing – review & editing, Methodology. **Shaaz Ghouse:** Methodology, Conceptualization. **Jonathan R.T Jeffers:** Writing – review & editing, Supervision, Project administration, Funding acquisition, Conceptualization.

Declaration of Competing Interest

The authors declare that they have no known competing financial interests or personal relationships that could have appeared to influence

the work reported in this paper.

Acknowledgements

The authors wish to gratefully acknowledge the Engineering and Physical Sciences Research Council, UK (EP/R042721/1), National Institute for Health Research, UK (NIHR300013) and Renishaw PLC, UK for their financial and technical support of this study.

Appendix A. Supporting information

Supplementary data associated with this article can be found in the online version at [doi:10.1016/j.addma.2022.102730](https://doi.org/10.1016/j.addma.2022.102730).

References

- [1] M.F. Ashby, The properties of foams and lattices, *Philos. Trans. R. Soc. A Math. Phys. Eng. Sci.* 364 (2006) 15–30, <https://doi.org/10.1098/rsta.2005.1678>.
- [2] L.J. Gibson, M.F. Ashby, *Cellular Solids*, Cambridge University Press, 1997, <https://doi.org/10.1017/CBO9781139878326>.
- [3] A.A. Zadpoor, Mechanical performance of additively manufactured meta-biomaterials, *Acta Biomater.* 85 (2019) 41–59, <https://doi.org/10.1016/j.actbio.2018.12.038>.
- [4] B. Subia, J. Kundu, S. C. Biomaterial Scaffold Fabrication Techniques for Potential Tissue Engineering Applications, in: *Tissue Eng. InTech*, 2010, <https://doi.org/10.5772/8581>.
- [5] T. Maconachie, M. Leary, B. Lozanovski, X. Zhang, M. Qian, O. Faruque, M. Brandt, SLM lattice structures: properties, performance, applications and challenges, *Mater. Des.* 183 (2019), 108137, <https://doi.org/10.1016/j.matdes.2019.108137>.
- [6] C. Pan, Y. Han, J. Lu, Design and optimization of lattice structures: a review, *Appl. Sci.* 10 (2020), <https://doi.org/10.3390/app10186374>.
- [7] S.J. Li, L.E. Murr, X.Y. Cheng, Z.B. Zhang, Y.L. Hao, R. Yang, F. Medina, R. B. Wicker, Compression fatigue behavior of Ti–6Al–4V mesh arrays fabricated by electron beam melting, *Acta Mater.* 60 (2012) 793–802, <https://doi.org/10.1016/J.ACTAMAT.2011.10.051>.
- [8] S.J. Li, Q.S. Xu, Z. Wang, W.T. Hou, Y.L. Hao, R. Yang, L.E. Murr, Influence of cell shape on mechanical properties of Ti–6Al–4V meshes fabricated by electron beam melting method, *Acta Biomater.* 10 (2014) 4537–4547, <https://doi.org/10.1016/J.ACTBIO.2014.06.010>.
- [9] S. Amirkhani, R. Bagheri, A. Zehtab Yazdi, Manipulating failure mechanism of rapid prototyped scaffolds by changing nodal connectivity and geometry of the pores, *J. Biomech.* 45 (2012) 2866–2875, <https://doi.org/10.1016/j.jbiomech.2012.08.029>.
- [10] A. Gross, P. Pantidis, K. Bertoldi, S. Gerasimidis, Correlation between topology and elastic properties of imperfect truss-lattice materials, *J. Mech. Phys. Solids* 124 (2019) 577–598, <https://doi.org/10.1016/j.jmps.2018.11.007>.
- [11] R. Hedayati, S.M. Ahmadi, K. Lietaert, B. Pouran, Y. Li, H. Weinans, C.D. Rans, A. A. Zadpoor, Isolated and modulated effects of topology and material type on the mechanical properties of additively manufactured porous biomaterials, *J. Mech. Behav. Biomed. Mater.* 79 (2018) 254–263, <https://doi.org/10.1016/J.JMBBM.2017.12.029>.
- [12] S.M. Ahmadi, S.A. Yavari, R. Wauthle, B. Pouran, J. Schrooten, H. Weinans, A. A. Zadpoor, Additively manufactured open-cell porous biomaterials made from six different space-filling unit cells: The mechanical and morphological properties, *Mater. (Basel)* 8 (2015) 1871–1896, <https://doi.org/10.3390/ma8041871>.
- [13] D. Zhao, Y. Huang, Y. Ao, C. Han, Q. Wang, Y. Li, J. Liu, Q. Wei, Z. Zhang, Effect of pore geometry on the fatigue properties and cell affinity of porous titanium scaffolds fabricated by selective laser melting, *J. Mech. Behav. Biomed. Mater.* 88 (2018) 478–487, <https://doi.org/10.1016/j.jmbbm.2018.08.048>.
- [14] S.M. Ahmadi, R. Hedayati, Y. Li, K. Lietaert, N. Tümer, A. Fatemi, C.D. Rans, B. Pouran, H. Weinans, A.A. Zadpoor, Fatigue performance of additively manufactured meta-biomaterials: the effects of topology and material type, *Acta Biomater.* 65 (2018) 292–304, <https://doi.org/10.1016/J.ACTBIO.2017.11.014>.
- [15] V.S. Deshpande, M.F. Ashby, N.A. Fleck, Foam topology: bending versus stretching dominated architectures, *Acta Mater.* 49 (2001) 1035–1040, [https://doi.org/10.1016/S1359-6454\(00\)00379-7](https://doi.org/10.1016/S1359-6454(00)00379-7).
- [16] M. Munford, U. Hossain, S. Ghouse, J.R.T. Jeffers, Prediction of anisotropic mechanical properties for lattice structures, *Addit. Manuf.* 32 (2020), 101041, <https://doi.org/10.1016/j.addma.2020.101041>.
- [17] U. Hossain, S. Ghouse, K. Nai, J.R. Jeffers, Controlling and testing anisotropy in additively manufactured stochastic structures, *Addit. Manuf.* 39 (2021), <https://doi.org/10.1016/j.addma.2021.101849>.
- [18] J. Mueller, K.H. Matlack, K. Shea, C. Daraio, Energy Absorption Properties of Periodic and Stochastic 3D Lattice Materials, *Adv. Theory Simul.* 2 (2019) 1–11, <https://doi.org/10.1002/adts.201900081>.
- [19] S. Raghavendra, A. Molinari, A. Cao, C. Gao, F. Berto, G. Zappini, M. Benedetti, Quasi-static compression and compression-compression fatigue behavior of regular and irregular cellular biomaterials, *Fatigue Fract. Eng. Mater. Struct.* 44 (2021) 1178–1194, <https://doi.org/10.1111/ffe.13422>.
- [20] Z. Wang, C. Wang, C. Li, Y. Qin, L. Zhong, B. Chen, Z. Li, H. Liu, F. Chang, J. Wang, Analysis of factors influencing bone ingrowth into three-dimensional printed porous metal scaffolds: a review, *J. Alloy. Compd.* 717 (2017) 271–285, <https://doi.org/10.1016/j.jallcom.2017.05.079>.
- [21] S. Ghouse, N. Reznikov, O.R. Boughton, S. Babu, K.C.G. Ng, G. Blunn, J.P. Cobb, M. M. Stevens, J.R.T. Jeffers, The design and in vivo testing of a locally stiffness-matched porous scaffold, *Appl. Mater. Today* 15 (2019), <https://doi.org/10.1016/j.apmt.2019.02.017>.
- [22] J. Henkel, M.A. Woodruff, D.R. Epari, R. Steck, V. Glatt, I.C. Dickinson, P.F. M. Choong, M.A. Schuetz, Di.W. Hutmacher, Bone Regeneration Based on Tissue Engineering Conceptions-A 21st Century Perspective, *Bone Res* 1 (2013) 216–248, <https://doi.org/10.4248/BR201303002>.
- [23] E.F. Morgan, H.H. Bayraktar, T.M. Keaveny, Trabecular bone modulus-density relationships depend on anatomic site, *J. Biomech.* 36 (2003) 897–904, [https://doi.org/10.1016/S0021-9290\(03\)00071-X](https://doi.org/10.1016/S0021-9290(03)00071-X).
- [24] Y. Yang, Y. Cheng, S. Peng, L. Xu, C. He, F. Qi, M. Zhao, C. Shuai, Microstructure evolution and texture tailoring of reduced graphene oxide reinforced Zn scaffold, *Bioact. Mater.* 6 (2021) 1230–1241, <https://doi.org/10.1016/J.BIOACTMAT.2020.10.017>.
- [25] S. Van Bael, Y.C. Chai, S. Truscello, M. Moesen, G. Kerckhofs, H. Van Oosterwyck, J.P. Kruth, J. Schrooten, The effect of pore geometry on the in vitro biological behavior of human periosteum-derived cells seeded on selective laser-melted Ti6Al4V bone scaffolds, *Acta Biomater.* 8 (2012) 2824–2834, <https://doi.org/10.1016/j.actbio.2012.04.001>.
- [26] S. Ghouse, S. Babu, R.J. Van Arkel, K. Nai, P.A. Hooper, J.R.T. Jeffers, The influence of laser parameters and scanning strategies on the mechanical properties of a stochastic porous material, *Mater. Des.* 131 (2017), <https://doi.org/10.1016/j.matdes.2017.06.041>.
- [27] S. Ghouse, S. Babu, K. Nai, P.A. Hooper, J.R.T. Jeffers, The influence of laser parameters, scanning strategies and material on the fatigue strength of a stochastic porous structure, *Addit. Manuf.* 22 (2018) 290–301, <https://doi.org/10.1016/j.addma.2018.05.024>.
- [28] R.N. Oosterbeek, *StrutSurf v1.0*, (2021). <https://doi.org/10.5281/zenodo.5785687>.
- [29] International Organization for Standardization, ISO 13314:2011 Mechanical testing of metals – Ductility testing – Compression test for porous and cellular metals (ISO Standard No. 13314:2011(E)), (2011).
- [30] International Organization for Standardization, BS ISO 1099: 2017 BSI Standards Publication Metallic materials — Fatigue testing — Axial force-controlled method, (2017).
- [31] S. Amin Yavari, R. Wauthle, J. Van Der Stok, A.C. Riemslag, M. Janssen, M. Mulier, J.P. Kruth, J. Schrooten, H. Weinans, A.A. Zadpoor, Fatigue behavior of porous biomaterials manufactured using selective laser melting, *Mater. Sci. Eng. C* 33 (2013) 4849–4858, <https://doi.org/10.1016/j.msec.2013.08.006>.
- [32] F. Li, J. Li, T. Huang, H. Kou, L. Zhou, Compression fatigue behavior and failure mechanism of porous titanium for biomedical applications, *J. Mech. Behav. Biomed. Mater.* 65 (2017) 814–823, <https://doi.org/10.1016/j.jmbbm.2016.09.035>.
- [33] International Organization for Standardization, ISO 12107:2012(E) Metallic materials — Fatigue testing — Statistical planning and analysis of data, (2012).
- [34] S. Ghouse, R.N. Oosterbeek, A.T. Mehmood, F. Vecchiato, D. Dye, J.R.T. Jeffers, Vacuum heat treatments of titanium porous structures, *Addit. Manuf.* 47 (2021), 102262, <https://doi.org/10.1016/j.addma.2021.102262>.
- [35] M. Baier, M. Sinico, A. Witvrouw, W. Dewulf, S. Carmignato, A novel tomographic characterisation approach for sag and gross defects in metal additively manufactured channels, *Addit. Manuf.* 39 (2021), 101892, <https://doi.org/10.1016/J.ADDMA.2021.101892>.
- [36] M. Leary, M. Mazur, H. Williams, E. Yang, A. Alghamdi, B. Lozanovski, X. Zhang, D. Shidid, L. Farahbod-Sternahl, G. Witt, I. Kelbassa, P. Choong, M. Qian, M. Brandt, Inconel 625 lattice structures manufactured by selective laser melting (SLM): mechanical properties, deformation and failure modes, *Mater. Des.* 157 (2018) 179–199, <https://doi.org/10.1016/J.MATDES.2018.06.010>.
- [37] M. Vesnjak, C. Veyhl, T. Fiedler, Analysis of anisotropy and strain rate sensitivity of open-cell metal foam, *Mater. Sci. Eng. A* 541 (2012) 105–109, <https://doi.org/10.1016/J.MSEA.2012.02.010>.
- [38] M. Ashby, A. Evans, N. Fleck, L. Gibson, J. Hutchinson, H. Wadley, F. Delale, Metal foams: a design guide, *Appl. Mech. Rev.* 54 (2001) B105–B106, <https://doi.org/10.1115/1.1421119>.
- [39] M. Mazur, M. Leary, S. Sun, M. Vcelka, D. Shidid, M. Brandt, Deformation and failure behaviour of Ti-6Al-4V lattice structures manufactured by selective laser melting (SLM), *Int. J. Adv. Manuf. Technol.* 84 (2016) 1391–1411, <https://doi.org/10.1007/s00170-015-7655-4>.
- [40] S. Arabnejad, R. Burnett Johnston, J.A. Pura, B. Singh, M. Tanzer, D. Pasini, High-strength porous biomaterials for bone replacement: a strategy to assess the interplay between cell morphology, mechanical properties, bone ingrowth and manufacturing constraints, *Acta Biomater.* 30 (2016) 345–356, <https://doi.org/10.1016/J.ACTBIO.2015.10.048>.
- [41] N.W. Hrabec, P. Heinel, B. Flinn, C. Körner, R.K. Bordia, Compression-compression fatigue of selective electron beam melted cellular titanium (Ti-6Al-4V), *J. Biomed. Mater. Res. Part B Appl. Biomater.* 99 B (2011) 313–320, <https://doi.org/10.1002/jbm.b.31901>.
- [42] R. Wauthle, S.M. Ahmadi, S. Amin Yavari, M. Mulier, A.A. Zadpoor, H. Weinans, J. Van Humbeeck, J.P. Kruth, J. Schrooten, Revival of pure titanium for dynamically loaded porous implants using additive manufacturing, *Mater. Sci. Eng. C* 54 (2015) 94–100, <https://doi.org/10.1016/J.MSEC.2015.05.001>.
- [43] F. Li, J. Li, H. Kou, L. Zhou, Porous Ti6Al4V alloys with enhanced normalized fatigue strength for biomedical applications, *Mater. Sci. Eng. C* 60 (2016) 485–488, <https://doi.org/10.1016/j.msec.2015.11.074>.

- [44] B. Van Hooreweder, Y. Apers, K. Lietaert, J.P. Kruth, Improving the fatigue performance of porous metallic biomaterials produced by selective laser melting, *Acta Biomater.* 47 (2017) 193–202, <https://doi.org/10.1016/j.actbio.2016.10.005>.
- [45] K. Karami, A. Blok, L. Weber, S.M. Ahmadi, R. Petrov, K. Nikolic, E.V. Borisov, S. Leeftang, C. Ayas, A.A. Zadpoor, M. Mehdipour, E. Reinton, V.A. Popovich, Continuous and pulsed selective laser melting of Ti6Al4V lattice structures: effect of post-processing on microstructural anisotropy and fatigue behaviour, *Addit. Manuf.* 36 (2020), 101433, <https://doi.org/10.1016/j.addma.2020.101433>.
- [46] B. Van Hooreweder, J.P. Kruth, Advanced fatigue analysis of metal lattice structures produced by selective laser melting, *CIRP Ann. Manuf. Technol.* 66 (2017) 221–224, <https://doi.org/10.1016/j.cirp.2017.04.130>.
- [47] N. Reznikov, O.R. Boughton, S. Ghouse, A.E. Weston, L. Collinson, G.W. Blunn, J.R. T. Jeffers, J.P. Cobb, M.M. Stevens, Individual response variations in scaffold-guided bone regeneration are determined by independent strain- and injury-induced mechanisms, *Biomaterials* 194 (2019), <https://doi.org/10.1016/j.biomaterials.2018.11.026>.
- [48] J. Wieding, A. Wolf, R. Bader, Numerical optimization of open-porous bone scaffold structures to match the elastic properties of human cortical bone, *J. Mech. Behav. Biomed. Mater.* 37 (2014) 56–68, <https://doi.org/10.1016/J.JMBBM.2014.05.002>.
- [49] F. Liu, Z. Mao, P. Zhang, D.Z. Zhang, J. Jiang, Z. Ma, Functionally graded porous scaffolds in multiple patterns: new design method, physical and mechanical properties, *Mater. Des.* 160 (2018) 849–860, <https://doi.org/10.1016/J.MATDES.2018.09.053>.
- [50] X.Y. Zhang, G. Fang, L.L. Xing, W. Liu, J. Zhou, Effect of porosity variation strategy on the performance of functionally graded Ti-6Al-4V scaffolds for bone tissue engineering, *Mater. Des.* 157 (2018) 523–538, <https://doi.org/10.1016/J.MATDES.2018.07.064>.